Single-Phase On-Board Bidirectional PEV Charger for V2G Reactive Power Operation

Mithat C. Kisacikoglu, *Member, IEEE,* Metin Kesler, *Member, IEEE,* and Leon M. Tolbert, *Fellow, IEEE*

***Abstract*—This paper presents the design and implementation of a single-phase on-board bidirectional plug-in electric vehicle (PEV) charger that can provide reactive power support to the utility grid in addition to charging the vehicle battery. The topology consists of two-stages: 1) a full-bridge ac–dc boost converter; and 2) a half-bridge bidirectional dc–dc converter. The charger operates in two quadrants in the active-reactive power (PQ) power plane with five different operation modes (i.e., charging-only, charging-capacitive, charging-inductive, capacitive-only, and inductive-only). This paper also presents a unified controller to follow utility PQ commands in a smart grid environment. The cascaded two-stage system controller receives active and reactive power commands from the grid, and results in line current and battery charging current references while also providing a stable dynamic response. The vehicle's battery is not affected during reactive power operation in any of the operation modes. Testing the unified system controller with a 1.44 kVA experimental charger design demonstrates the successful implementation of reactive power support functionality of PEVs for future smart grid applications.**

***Index Terms*—Battery charger, plug-in electric vehicle (PEV), reactive power, vehicle-to-grid (V2G).**

I. Introduction

PLUG-IN electric vehicle (PEV) sales are expected to increase in the coming years as a cost-effective alternative to conventional internal combustion engine (ICE) vehicles. PEVs present a more efficient operation and, thereby, have increased fuel cost savings [1]. However, large number of PEV connection to the electricity network raises concerns about reliability of the grid especially at the low voltage distribution network due to substantial increase in the peak load [2], [3]. Smart and coordinated charging of the PEVs will alleviate the negative impact on the grid. Furthermore, PEVs can also serve as distributed energy storage units utilizing the readily available on-board charger which would further benefit to the utility grid [4], [5].

On-board chargers convert the ac grid voltage into dc, and they typically have unidirectional power transfer capability. Using a more advanced topology and controller compared to conventional methods available in the market, the on-board charger can also supply power quality functions such as reactive power compensation (inductive or capacitive), voltage regulation, harmonic filtering, and power factor correction [6]–[10].

Today, in the utility grid, reactive power consumed at the residential load is compensated using capacitor banks, static VAR compensators, static synchronous compensators, etc. However, compensation of the reactive power very close to the residential load is more efficient and reduces the installation and maintenance costs associated with the aforementioned devices. Therefore, on-board chargers could be suited to support advanced functions with limited modifications to the conventional topologies. Furthermore, reactive power support does not affect the battery state of charge (SoC) or battery lifetime. The ac–dc converter losses during reactive power compensation is supplied by the utility grid and, therefore, battery SoC is preserved. However, it is important to note that reactive power operation affects components such as dc-link capacitors since more charge-discharge cycles take place [6].

Considering its benefits, smart charging with vehicle-to-grid (V2G) has been found advantageous and attractive in the long term operation of the electricity grid [5], [11]. In the future, utilities would want to communicate PEV charging power with the customer and control it with an incentive in return [5], [11]–[13]. With increasing interest in V2G applications for the utility grid, studies have investigated stand-alone and grid support operation modes of battery supplied bidirectional converters [6]–[10], [14]–[19].

In general, a two stage topology with cascaded ac–dc converter and dc–dc converter is proposed in the literature for bidirectional battery charger operation due to two main reasons: 1) to implement galvanic isolation; and 2) to decrease second harmonic (2-f) ripple component in the dc battery charging current to protect lithium-ion (Li-ion) battery lifetime. 2-f ripple is the natural byproduct of single phase ac–dc rectification of the power [20]. In [8], [9], [16], and [18], two separate controllers are commonly used for ac–dc and dc–dc converter stages. Therefore, controller uses separate references for ac–dc and dc–dc stages (i.e., P_{cmd}, Q_{cmd},

Manuscript received February 27, 2014; revised July 21, 2014; accepted September 6, 2014. Date of publication October 15, 2014; date of current version February 16, 2015. This work was supported in part by the Engineering Research Center Program of the National Science Foundation (NSF), in part by the Department of Energy under NSF Award EEC-1041877, in part by the CURENT Industry Partnership Program, and in part by the Scientific and Technological Research Council of Turkey 2219 and 2232 Award Programs. Paper no. TSG-00158-2014.

M. C. Kisacikoglu is with the Department of Electrical and Electronics Engineering, College of Engineering, Hacettepe University, Ankara 06800, Turkey (e-mail: mkisacik@hacettepe.edu.tr).

M. Kesler is with the Department of Computer Engineering, Bilecik Seyh Edebali University, Bilecik 11210, Turkey.

L. M. Tolbert is with the Department of Electrical Engineering and Computer Science, University of Tennessee, Knoxville, TN 37996-2250 USA; and also with Oak Ridge National Laboratory, Oak Ridge TN 37381, TN, USA.

Color versions of one or more of the figures in this paper are available online at http://ieeexplore.ieee.org.

Digital Object Identifier 10.1109/TSG.2014.2360685

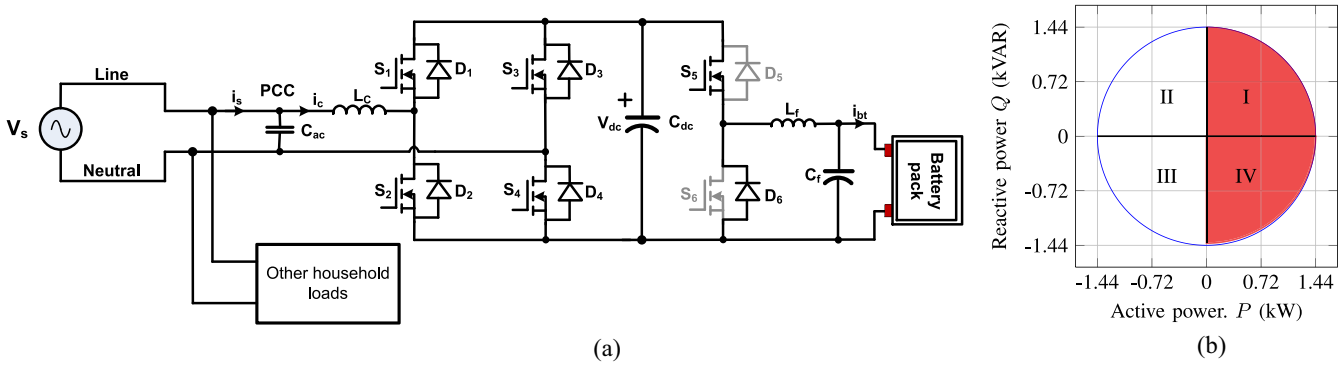

Fig. 1. Bidirectional PEV charger and its operation region in active-reactive power (PQ) plane. (a) Charger and grid connection. (b) Operation area of the charger (shaded).

and i_{bt}^*). However, a uniform controller that would only communicate active power command (P_{cmd}) and reactive power command (Q_{cmd}) [or power factor (pf)] between EV and utility grid is more feasible for a smart-grid connection due to physical interoperability [21]. It is more feasible and standardized to communicate two signals (P_{cmd} and Q_{cmd}) to the utility grid and derive other references from those signals.

In [10], [17], and [22], a uniform controller is used that responds P_{cmd} and Q_{cmd} signals from the grid as proposed in this paper. Moreover, P_{cmd} is used as the reference for dc battery charging power, and ac–dc converter regulates the dc-link voltage and tracks Q_{cmd}. As a result, P_{cmd} is not the reference for the actual active power (P) measured at the point of common coupling (PCC). This introduces a power mismatch (between P_{cmd} and P) because of neglecting the losses in active and passive devices of ac–dc converter. However, active power at the PCC must follow P_{cmd} from the utility grid, and the controller should derive the required battery reference current (i_{bt}) that is needed to respond P_{cmd}.

In addition, bidirectional operation in the above mentioned studies do not explicitly shows the controller performance on how fast charger responds to Q_{cmd} or P_{cmd} variations. A cascaded system controller demonstration should be performed to help system integration analysis of PEV V2G applications. Therefore, a unified system controller is preferred in which the utility grid only sends two signals (P_{cmd} and Q_{cmd}) and expects the charger to follow those commands.

This paper proposes a control strategy for a bidirectional on-board charger to utilize it for battery charging and reactive power operation support. The system controller unifies the ac–dc and dc–dc converter control, and fulfills P_{cmd} and Q_{cmd} transmitted between the PEV and the utility grid. The proposed control strategy is first developed in powersim (PSIM), and then a 1.44 kVA bench-top on-board charger is designed and tested to show the controller performance. The dynamic performance and steady-state operation tests of the on-board charging system are realized in simulation and in the experimental prototype. The results show that the proposed control method operates successfully providing good dynamic response under grid demand variations, and meets steady-state operation conditions.

Section II describes the charger system and charger design requirements. Section III is concerned with the proposed system controller development. Section IV focuses on simulation verification of the proposed system controller. Section V demonstrates the experimental results of the proposed system controller utilizing a Level 1 grid connection.

II. System Description of the Bidirectional PEV Charger

The topology used in this paper to investigate the PEV-grid interaction is shown in Fig. 1(a). The PEV on-board chargers typically include two stages: 1) the ac–dc rectification (i.e., full-bridge ac–dc rectifier) and 2) dc–dc conversion (i.e., dc–dc buck converter). Practical applications usually require galvanic isolation. However, this paper employs a non-isolated topology. The focus of this paper is to implement charging and reactive power control at the same time with meeting the design requirements (which are presented in the system description). Therefore, most of the effort has been on the controller design and implementation, and on the analysis of the experimental results.

Bipolar modulation is used for the front-end ac–dc converter, meaning that the rectifier input voltage is either $+V_{\text{dc}}$ or $-V_{\text{dc}}$. When S_1 and S_4 are on, switches S_2 and S_3 are turned off, and vice versa. The peak voltage that the metal-oxide-semiconductor field-effect transistors (MOSFETs) and diodes block is equal to V_{dc}, and the peak current they need to conduct is equal to $\sqrt{2}I_c$ where I_c is the charger rms current.

The battery voltage level used in PEVs usually ranges between 200 and 390 V [1]. Therefore, two different dc-link voltage levels [V_{dc} in Fig. 1(a)] are tested in this paper: 1) 250 and 2) 400 V. The buck operation is achieved using switch S_5 and D_6. When S_5 is turned on, the current flows through S_5 and L_f, and charges C_f and the battery. When S_5 is turned off, diode D_6 conducts the free-wheeling inductor current through inductor L_f and battery while C_f is discharged into the battery. The switches S_6 and D_5 are not used in this paper since the battery is not discharged. However, the system hardware is implemented for V2G active power applications. The system parameters of Fig. 1(a) are listed in Table I.

The grid current (i_s) must have a total harmonic distortion (THD) less than 5% and the individual harmonic components must also be well regulated [23], [24]. This is achieved by using an inductor-capacitor filter at the front end

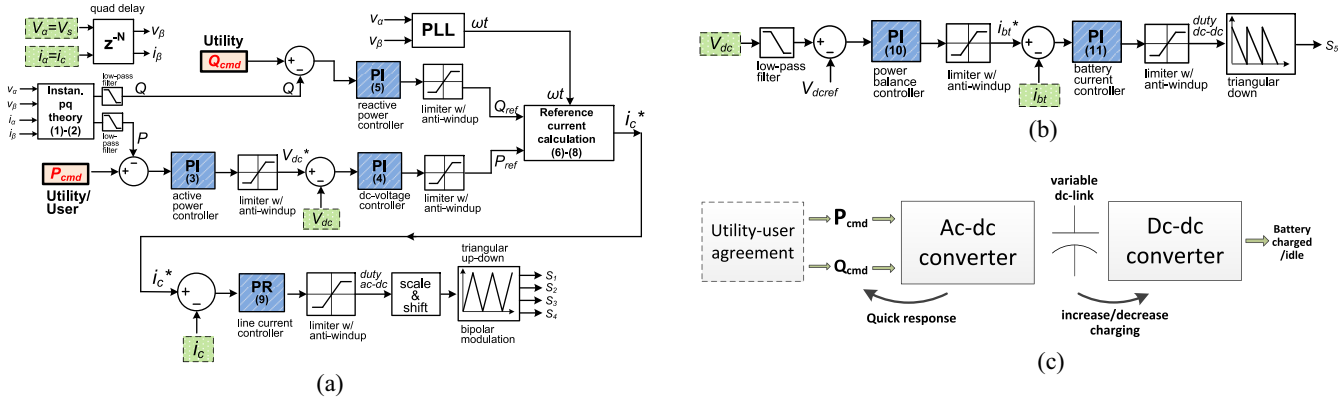

Fig. 2. Proposed system controller and operation. Controller for (a) ac–dc converter and (b) dc–dc converter. (c) Controller operation sequence.

TABLE I
SYSTEM PARAMETERS USED IN THIS PAPER

Parameter	Symbol	Value
Charger apparent power	S	1.44 kVA
Grid voltage	V_s	120 V
Grid frequency	f	60 Hz
Coupling inductance	L_c	1.0 mH
AC-DC converter switching frequency	f_{sw1}	24 kHz
DC-link voltage	V_{dc}	250 V/ 400 V
DC-link capacitance	C_{dc}	330 μF
DC-DC converter switching frequency	f_{sw2}	42 kHz
Battery side filter capacitor	C_f	200 μF
Battery side filter inductance	L_f	400 μH

TABLE II
LIST OF CONTROLLER PARAMETERS

Parameter	Equat. Ref. #	Symbol	Value
Angular frequency	(8), (9)	ω	377 rad/s
Crossover angular frequency	(9)	ω_c	3.0 rad/s
Proportional const. for PR contr. (i-loop)	(9)	K_p^c	0.6
Integral const. for PR contr. (i-loop)	(9)	K_i^c	500
Proportional const. for PI contr. (v-loop)	(4)	K_p^v	1.50
Integral const. for PI contr. (v-loop)	(4)	K_i^v	100
Proportional const. for PI contr. (Q-loop)	(5)	K_p^q	0.1
Integral const. for PI contr. (Q-loop)	(5)	K_i^q	30
Proportional const. for PI contr. (P-loop)	(3)	K_p^p	1.0
Integral const. for PI contr. (P-loop)	(3)	K_i^p	20
Proportional const. for PI contr. (Balance-loop)	(10)	K_p^{bl}	0.045
Integral const. for PI contr. (Balance-loop)	(10)	K_i^{bl}	0.50
Proportional const. for PI contr. (ibt-loop)	(11)	K_p^{ibt}	0.01
Integral const. for PI contr. (ibt-loop)	(11)	K_i^{ibt}	10

and by appropriately designing the ac inductor current feedback controller. The charger's output voltage and current are regulated using a low pass filter at the output and by tuning the output current (i_{bt}) controller parameters. Some of the employed practices for Li-ion and/or lead-acid batteries are charging rms current ripple of 5%–10% of the rated charging current and rms ripple voltage of 1.5% of the rated battery voltage [25].

III. CONTROLLER DESIGN OF THE BIDIRECTIONAL PEV CHARGER

In this paper, the charger operates in quadrant I and IV of the active-reactive power (PQ) power plane shown in Fig. 1(b). Therefore, there is no active power sent to the grid. Note, that active power and reactive power that are sent from the grid to the charger have positive sign and vice versa. P and Q in Fig. 1(b) are measured at the PCC shown in Fig. 1(a). The controller must ensure that the bidirectional charger can track active and reactive power commands provided that it operates in the region shown in Fig. 1(b).

The system has two interrelated controller subsections. One is for the ac–dc converter and the other is for the dc–dc converter [Fig. 2(a) and (b)].

Fig. 2(a) illustrates the proposed controller section for the ac–dc converter. The sensed signals (i_c, v_{dc}, and v_s) are shown within the dashed boxes. Orthogonal (β) axis components are generated using a delay function. One quarter of the grid period delay equals to $1/(60 \times 4)$ which corresponds to $N = 100$ samples with 24 kHz sampling frequency. The delayed signals are utilized for a single-phase phase-locked loop (PLL) algorithm which tracks the line voltage phase angle and generate the reference phase signal for the charger current [26]. Later, instantaneous pq theory developed for three-phase systems [27] is used to compute the single-phase active and reactive power. While sensed signals are used for α components ($v_\alpha = v_s$, $i_\alpha = i_c$), the signals are delayed for one-quarter to generate β components (v_β, i_β). Therefore,

$$P = \frac{1}{2}\left(v_\alpha \times i_\alpha + v_\beta \times i_\beta\right) \tag{1}$$

$$Q = -\frac{1}{2}\left(v_\alpha \times i_\beta + v_\beta \times i_\alpha\right). \tag{2}$$

Moreover, two low-pass filters are utilized for both of the outputs of (1) and (2) to yield P and Q.

The controller meets the required charging power command (P_{cmd}) from the customer. The utility can also control P_{cmd} to coordinate charging power during the peak hours. In this case, the utility must return an incentive to the customer. Also, if any reactive power is requested, the utility sends a reactive power command (Q_{cmd}) for the controller to follow. Depending on the agreement with the utility grid, P_{cmd} and Q_{cmd} must be processed before being sent to the charger.

The controller blocks are explained in the following equations. All the corresponding parameters are listed in Table II. All the equations are referred to Fig. 2(a) and (b) with corresponding equation numbers.

The most outer loop of the ac–dc controller is the power loop (P-loop) that is used to satisfy active power

command (P_{cmd}) by modifying the set-point for the dc-link voltage (V_{dc}^*) temporarily

$$V_{\text{dc}}^* = K_p^P \times (P_{\text{cmd}} - P) + \frac{K_i^P}{s} \times (P_{\text{cmd}} - P). \quad (3)$$

The inner dc voltage loop (v-loop) is used to follow V_{dc}^*. The output of this loop is the reference tracking power level for the charger

$$P_{\text{ref}} = K_p^v \times \left(V_{\text{dc}}{}^* - V_{\text{dc}}\right) + \frac{K_i^v}{s} \times \left(V_{\text{dc}}{}^* - V_{\text{dc}}\right). \quad (4)$$

Similarly, the outer reactive power loop (Q-loop) is used to match the reactive power output of the charger with the reactive power command from the utility grid via a proportional and integral (PI) controller. The output of the Q-loop is an indication of the reactive power that the charger should supply/sink

$$Q_{\text{ref}} = K_p^Q \times (Q_{\text{cmd}} - Q) + \frac{K_i^Q}{s} \times (Q_{\text{cmd}} - Q). \quad (5)$$

The outputs of the v-loop and Q-loop are used to generate the reference charger current (i_c^*). It is calculated using P_{ref} and Q_{ref} calculated in (4) and (5) via the following equations:

$$\theta = \tan^{-1}\left(\frac{Q_{\text{ref}}}{P_{\text{ref}}}\right) \quad (6)$$

$$I_c = \frac{P_{\text{ref}}}{V_s \cos(\theta)} \quad (7)$$

and finally

$$i_c^* = \sqrt{2}\, I_c \sin(\omega t - \theta). \quad (8)$$

The most inner loop (i-loop) is controlled using a nonideal proportional and resonant (PR) controller [28], [29]. The error current between the sensed line current (i_c) and reference current ($i_c{}^*$) is fed into the PR controller. The output of the PR controller is utilized to generate the duty cycle (d) for the ac–dc converter. Therefore

$$d = K_p^c \times \left(i_c{}^* - i_c\right) + \frac{2K_i^c\, \omega_c\, s}{s^2 + 2\,\omega_c\, s + \omega^2} \times \left(i_c{}^* - i_c\right) \quad (9)$$

which concludes the ac–dc controller subsection.

Fig. 2(b) shows the controller for the dc–dc converter. The reference battery current (i_{bt}^*) is calculated by amplifying the error between the permanent reference dc-link voltage V_{dcref} and V_{dc} with a PI controller as

$$i_{bt}^* = K_p^{bl} \times (V_{\text{dc}} - V_{\text{dcref}}) + \frac{K_i^{bl}}{s} \times (V_{\text{dc}} - V_{\text{dcref}}). \quad (10)$$

This loop is used to complement the P-loop to satisfy the P_{cmd} from the utility grid. It does not compete against P-loop but helps it to achieve input–output power balance. Then, instantaneous battery current is regulated to realize constant current (CC) charging as

$$d_o = K_p^{bt} \times \left(i_{bt}^* - i_{bt}\right) + \frac{K_i^{bt}}{s} \times \left(i_{bt}^* - i_{bt}\right) \quad (11)$$

where d_o is the duty cycle for the dc–dc converter. All of the controllers in the system are equipped with anti-windup limiter to compensate for the accumulated error in control variables.

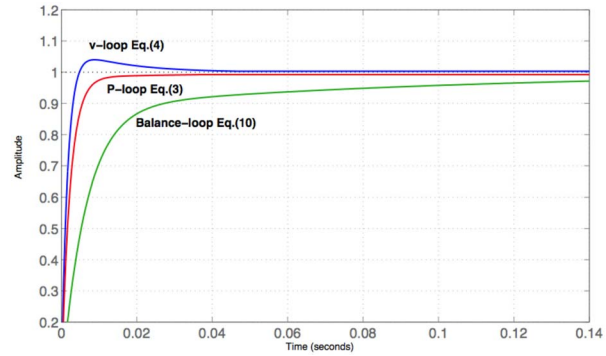

Fig. 3. Step responses of closed-loop controller transfer functions of (3), (4), and (10).

Due to having different loops, performance of the system is tested both in simulation and experiments at different steps. Controller design starts with designing inner ac inductor current (i_c) loop. Later, V_{dc} and then P-Q controller designs followed the i_c loop design. After closing the ac–dc converter controller loops, ac–dc converter is tested. The controller constants are finalized by parameter tuning to meet the desired performance.

DC–dc converter output current (i_{bt}) controller is designed and tested separately. Finally, power balance controller is tested after integrating ac–dc and dc–dc converters. Further parameter tuning is done after integration in power balance loop and battery current loop to meet system performance requirements.

The system employs a variable dc-link voltage control that generates battery reference current (i_{bt}^*) for the dc–dc stage. If P_{cmd} increases (decreases), V_{dc} increases (decreases) to a new set-point. This small increase (decrease) in V_{dc} yields an increase (decrease) in i_{bt}.

The dc-link voltage controller, given in (4), is dynamic with a fast-response characteristic compared to balance-loop given in (10). Moreover, (10) operates slower, and it satisfies power balance with a longer time constant. This provides a fast response at the PCC to the grid commands as illustrated in Fig. 2(c). DC–dc converter waits for the ac–dc converter response to the new operating point first, and then follows it by changing the battery current. The step responses of P-loop given in (3), v-loop given in (4), and balance-loop given in (10) are plotted in Fig. 3 using the parameters in Table II to show their response characteristics. Since, the bandwidth difference between (4) and (10) are large (about half a decade), two controllers do not conflict and the system operates without instability.

A low-pass filter is used after the dc-link voltage measurement for the dc–dc converter controller. It is aimed to filter 2-f components on the dc-link voltage when generating i_{bt}^*. The transfer function for the filter is as follows:

$$H(s) = \frac{k\,\omega_{c1}^2}{s^2 + 2\,\xi\,\omega_{c1}\, s + \omega_{c1}^2} \quad (12)$$

where $\omega_{c1} = 2\pi f_c$, $f_c = 20$ Hz, and $\xi = \sqrt{2}$.

TABLE III
SIMULATION SCENARIO

Operation Time	Active Power P_{cmd}, (kW)	Reactive Power Q_{cmd}, (kVAR)	Apparent Power S, (kVA)	Power Factor
1-3 s	1.44	0	1.44	1.0 unity
3-5 s	0.84	-1.12	1.44	0.6 leading
5-7 s	1.12	0.84	1.44	0.8 lagging

It is important to note that initial SoC and battery pack size of the PEV do not affect the controller performance. Different SoC levels have been tested and the resulting response to the power commands is verified to be similar.

Regardless of battery SoC, charger can draw nominal charging power as long as it is in CC charging mode. Battery SoC is observed by the battery management system (BMS) and charger switches to constant voltage (CV) charging when it finishes CC charging. In this paper, we only operated in CC charging region, which covers 80% of the energy capacity of the battery. Therefore, battery terminal voltage is not included in the controller design.

IV. SIMULATION VERIFICATION OF THE PROPOSED PEV CHARGER CONTROLLER

A simulation scenario is developed to show the operation of the charger and its response performance to the grid commands. Since, the required time to simulate the utility level operation of the charger is too long, a condensed version of the scenario is developed. It is assumed that the PEVs are plugged into the grid during peak hours (4:00–8:00 P.M.) when the load is at its highest level and the battery requires full charging. Therefore, the simulation starts with charging only operation. Then, it is expected that the voltage at the substation decreases as the reactive power and active power consumption at the residential units increases. The utility makes an action to support the distribution voltage by utilizing some of the PEVs for reactive power supply. Later, if the utility needs to decrease the substation voltage, the PEV can also consume reactive power. Table III lists the steps of this scenario in the given order. Table III is implemented with a 7-s simulation.

Fig. 4 shows the developed simulation diagram in PSIM. The proposed charger controller code is developed in C language and embedded into the system simulation structure. The PSIM Li-ion battery model is used in the simulation [30]. Necessary parameters are extracted from the data sheet of Li-ion batteries available in the laboratory [31]. The system parameters used in the simulation and shown in Table I are the same as the experimental hardware set-up that will be explained in the next section. The utility commands for active and reactive power are embedded into the C code and activated through a time counter mechanism to realize Table III. Simulation results provided very similar behavior with the real set-up during start-up and dynamic performance tests. Therefore, it provided a fast controller code development process and reduced implementation failures.

The simulation results are completed for two different cases. Since, the selection of the dc-link voltage depends on the battery pack voltage, controller performances are confirmed for $V_{\mathrm{dc}} = 250$ and 400 V. Fig. 5 shows the results for 400 V dc-link voltage. P and Q in the figure are the calculated active and reactive power outputs of the charger at the PCC. The controller followed the active and reactive power commands successfully. Note that, the charger current rms value ($I_c = 1440/120 = 12$ A) stays the same during the simulation since the apparent power is kept constant. The transitions from one mode to another are shown in further detail in Fig. 6. Settling time is less than five grid cycles for Fig. 6(a) and (b).

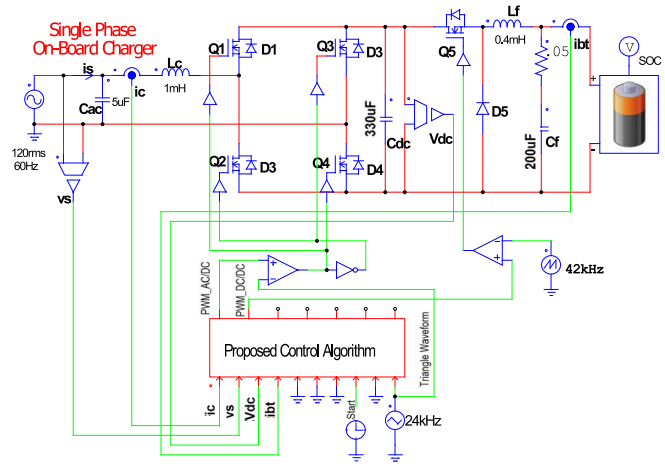

Fig. 4. Simulation diagram of the charger developed in PSIM.

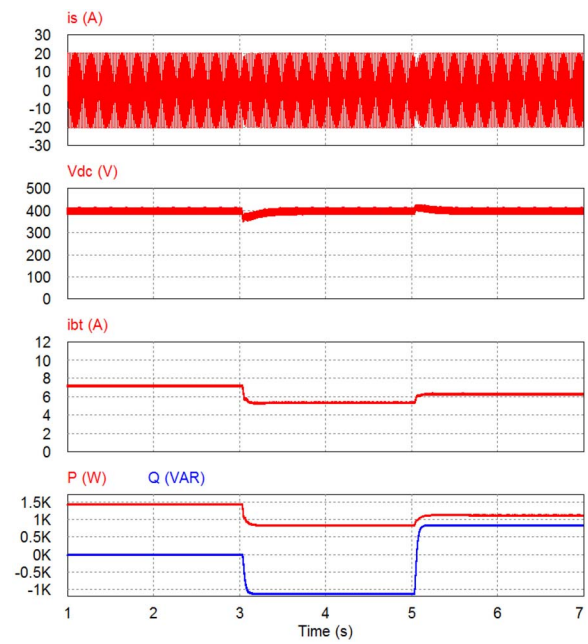

Fig. 5. Verification of the system controller using PSIM for 400 V dc-link voltage.

V. EXPERIMENTAL VERIFICATION OF THE PEV CHARGER FOR V2G REACTIVE POWER OPERATION

An experimental prototype has been developed to show the verification of the controller system design and to implement successful grid connection. The charger system is designed using a modular structure which provided flexibility in developing the system by allowing easy replacement of faulty

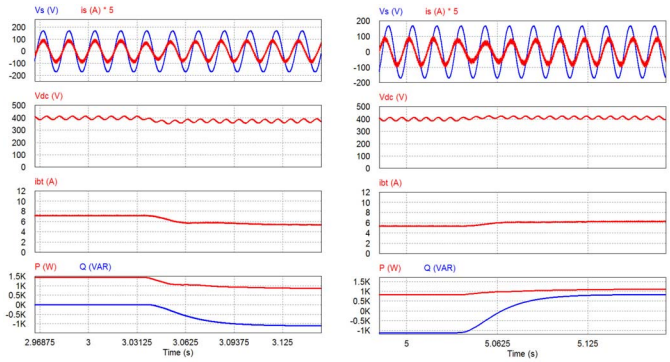

Fig. 6. Zoomed-in version of the simulation transients. Transition from (a) 1.0 unity pf to 0.6 leading pf and (b) 0.6 leading pf to 0.8 lagging pf.

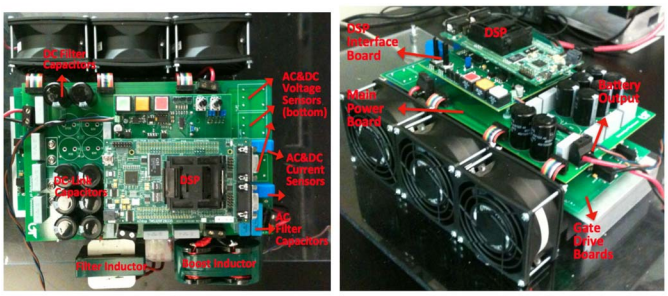

Fig. 7. Experimental prototype of the bidirectional PEV charger. (a) Top view. (b) Side view.

modules. The system is composed of three main units: 1) gate drive boards; 2) main power board; and 3) Digital signal processor (DSP) interface board for signal filtering and protection. Microsemi APT34M120J Si MOSFETs are used for the main power switches. A floating point Texas Instruments (TI) C2000 F28335 DSP is used for controller implementation. The experimental parameters of the system was presented in Table I. Aluminum dc-link capacitors (330 μF) are selected to have small volume in the final system. Fig. 7 shows the final configuration of the charger. As shown, the interface board and the DSP are placed very close to the sensors providing a short distance for the sensor-to-ADC traces.

The overall performance of the charger is tested using the simulation scenario for the verification of the controller's response of the active and reactive power commands as shown in Fig. 8. The system started from the arrow position, and it went into the operation modes in the order described in Table III [charging only, 0.6 pf leading (charging and capacitive operation), and 0.8 pf lagging (charging and inductive operation)]. P and Q in Fig. 8 stand for the measured active and reactive power at the PCC. Line current i_s, dc-link voltage $V_{\rm dc}$, and battery current i_{bt} are shown in Fig. 8. As the $P_{\rm cmd}$ increases, the dc-link voltage increases first and then so does the battery charging current and vice versa. The grid current amplitude stays the same through the experiment satisfying a maximum of 1.44 kVA power flow to the charger complying with a Level 1 connection. Overall,

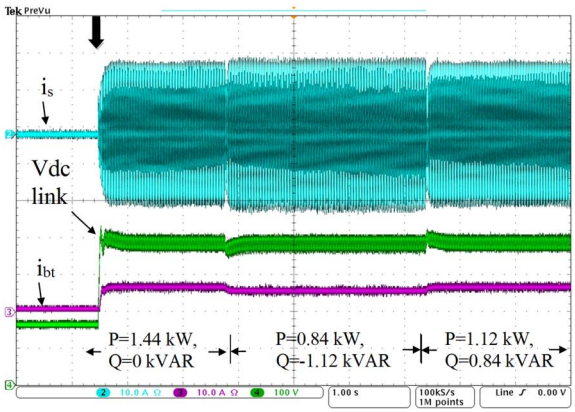

Fig. 8. Implemented experimental results of bidirectional PEV charger.

the experimental set-up performance confirmed the controller design.

Next, the start-up performance of the charger is presented in Fig. 9(a) to show the engagement and synchronization of the system with the grid. The charger started safely without drawing an excessive current from the grid. The dc-link voltage reaches the grid voltage peak value (169 V) when the charger is first plugged-in. At this time, there is no charging action and i_{bt} is zero. It does not draw grid current until the user starts the charging function [thick arrow in Fig. 9(a)]. Then, the dc-link voltage gradually increases to its rated value (400 V) and the charger draws full charging power which is 1.44 kW. There is a small overshoot in $V_{\rm dc}$ as predicted in Fig. 3. The grid current is in line with grid voltage satisfying unity pf operation.

Later, the transition periods between operation modes are explained and analyzed in detail. Fig. 9(b) shows the change in grid and battery currents when the charger receives a command change from 1.0 unity pf operation to 0.6 leading pf. This is a step change of ΔP = -42% on top of the full Q change. The transition time is less than five grid cycles as shown in Fig. 9(b) overlapping with simulation results. Battery current decreases to the new operating point at the end of the step change. The charger moves to new reactive power operation point without any problems. This verifies the increased effectiveness of supplying fast reactive power to the grid when needed via V2G.

The second test in Fig. 9(c) shows the change from 0.6 leading pf to 0.8 lagging pf when there is a need to consume reactive power in the grid. The corresponding changes are charging power from 0.84 to 1.12 kW and reactive power output from -1.12 to 0.84 kVAR at the same time. This is a change of ΔP = 33% in addition to the Q change. While, the grid current leads the grid voltage before the command arrives, the current lags the voltage eventually after the transition period. Again, the transition completes before five grid cycles which is also in line with simulation results. Note that, the grid current amplitude is almost unchanged and the transition occurs smoothly without distorting the charging current.

To further analyze the line current quality, Fig. 10(a) and (b) shows the harmonic content of the line current, i_s, when the charger operates at charging only operation at 1.44 kW.

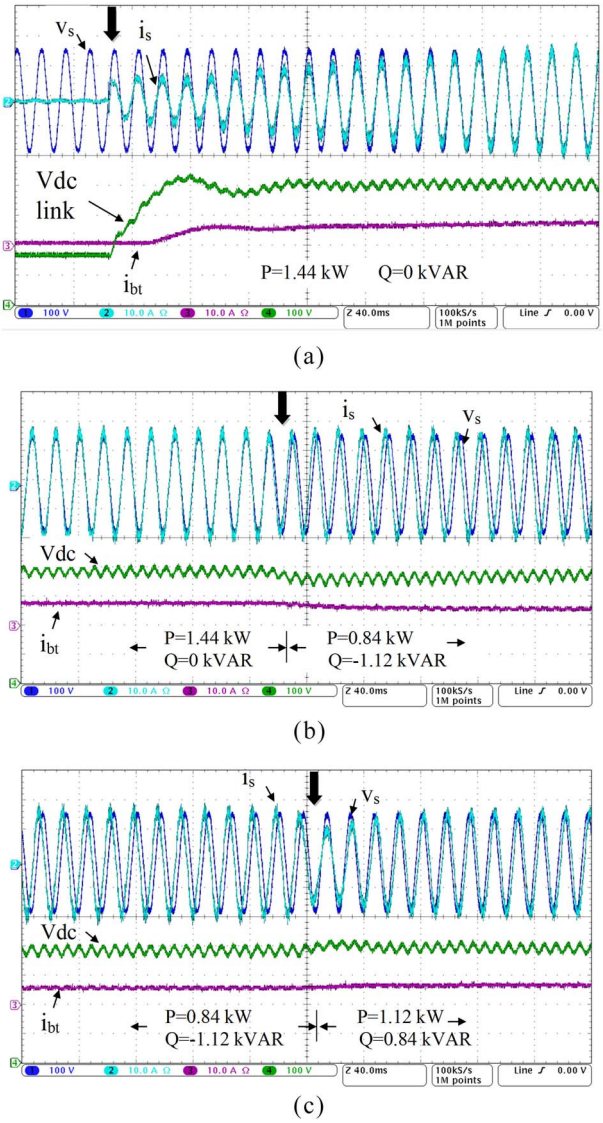

Fig. 9. Experimental results of the dynamic performance of the bidirectional charger. (a) From start-up to 1.44 kW charging only operation. (b) From 1.44 kW charging only operation to 0.84 kW charging and −1.12 kVAR reactive power operation. (c) From 0.84 kW charging and −1.12 kVAR reactive power to 1.12 kW charging and 0.84 kVAR reactive power operation.

They also show how it compares with the harmonics limits of IEC 61000-3-2 Class D and IEEE 519 standards [23], [24]. Odd harmonic components up to the order 33 are shown here, and the ones above are negligible. The total THD of the line current is measured to be 2.95% at 1.44 kW which complies with both of the standards. When compared with the IEC standards, the only failure in individual harmonics is observed at the 17th harmonic which is only slightly higher than the acceptable limit. On the other hand, the line current fulfills the IEEE 519 standard in individual harmonics. A total grid input-to-battery output efficiency of 92% is achieved at 1.44 kW measured with a Yokogawa PZ 4000 power analyzer.

Finally, Fig. 11 shows a summary of different operation modes to prove that the charger can operate effectively in the operation area illustrated in Fig. 1(b). The following operation modes are analyzed: 1) full inductive-only power; 2) full capacitive-only power; 3) full charging-only operation;

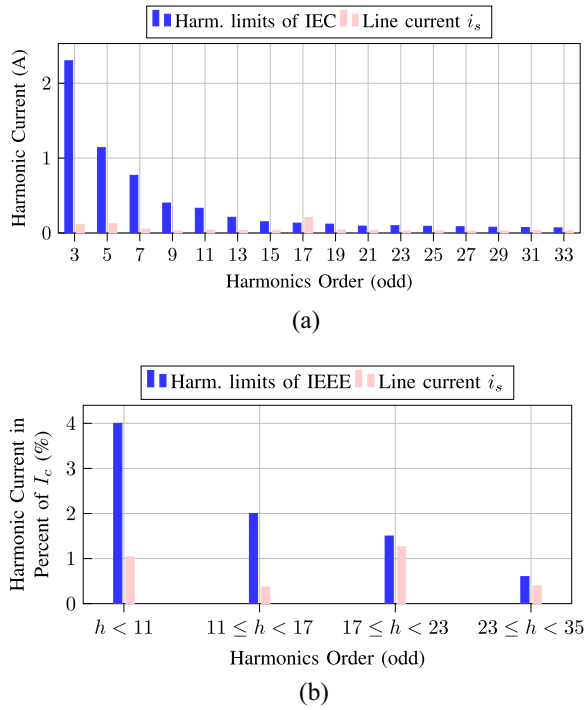

Fig. 10. Harmonic spectrum of the line current compared to the limits of (a) IEC 61000-3-2 Class D standard [24] and (b) IEEE 519 standard [23].

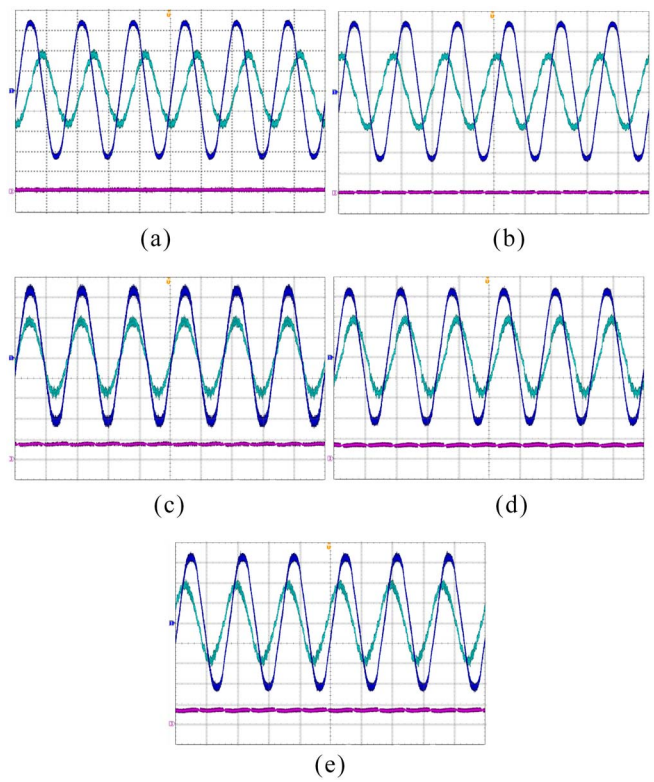

Fig. 11. Grid voltage $v_s(t)$, grid current $i_s(t)$, and battery current $i_{bt}(t)$ waveforms for each operation mode. (a) Mode#1-inductive operation. (b) Mode#2-capacitive operation. (c) Mode#3-charging operation. (d) Mode#4-charging and inductive operation. (e) Mode#5-charging and capacitive operation ($v_s(t)$: 50 V/div, $i_s(t)$: 10 A/div, $i_{bt}(t)$: 10 A/div, t: 10 ms/div).

4) 80% charging and 60% inductive power operation; and 5) 80% charging and 60% capacitive power operation. A total of six grid cycles (60 Hz) of grid voltage $v_s(t)$ and grid

current $i_s(t)$ are shown. The dc battery current $i_{bt}(t)$ is also illustrated at the bottom of each figure. Note that $i_{bt}(t)$ is close to zero when there is no charging power request, i.e., modes #1-#2. The designed controller operates in different operating modes without any stability problem. This shows that charger is suitable to take different roles for the sake of a more reliable utility grid.

VI. Conclusion

This paper focuses on controller development and experimental verification of charging and V2G reactive power operation using a single-phase on-board bidirectional charger. The proposed unified system controller receives charging active power and reactive power inputs from the utility grid and adjusts the line current and battery current without exceeding THD limits. It provides a fast dynamic response, along with a good steady-state performance.

The controller is tested utilizing a single-phase, Level 1, 120 V grid connection. However, the designed controller can also be applied at higher power levels in Level 2 single-phase charging. The battery is not affected from the reactive power operation either in terms of its lifetime or in available SoC. The controller fulfilled step-changes of inductive and capacitive reactive power commands in less than five grid cycles proving quick response to the utility commands. The simulation and experimental results show that the proposed PEV charger control method has a fast dynamic response, good steady-state performance, and operates successfully under grid demand variations.

Acknowledgment

The authors would like to thank Dr. B. Ozpineci from Oak Ridge National Laboratory.

References

[1] M. C. Kisacikoglu, A. Bedir, B. Ozpineci, and L. M. Tolbert, "PHEV-EV charger technology assessment with an emphasis on V2G operation," Oak Ridge Nat. Lab., Oak Ridge, TN, USA, Tech. Rep. ORNL/TM-2010/221, Mar. 2012.

[2] Z. Luo, Z. Hu, Y. Song, Z. Xu, and H. Lu, "Optimal coordination of plug-in electric vehicles in power grids with cost-benefit analysis-part I: Enabling techniques," *IEEE Trans. Power Syst.*, vol. 28, no. 4, pp. 3546–3555, Nov. 2013.

[3] D. Manz *et al.*, "The grid of the future: Ten trends that will shape the grid over the next decade," *IEEE Power Energy Mag.*, vol. 12, no. 3, pp. 26–36, May 2014.

[4] W. Kempton and S. E. Letendre, "Electric vehicles as a new power source for electric utilities," *Transp. Res.*, vol. 2, no. 3, pp. 157–175, 1997.

[5] Z. Luo, Z. Hu, Y. Song, Z. Xu, and H. Lu, "Optimal coordination of plug-in electric vehicles in power grids with cost-benefit analysis-part II: A case study in China," *IEEE Trans. Power Syst.*, vol. 28, no. 4, pp. 3556–3565, Nov. 2013.

[6] M. C. Kisacikoglu, B. Ozpineci, and L. M. Tolbert, "EV/PHEV bidirectional charger assessment for V2G reactive power operation," *IEEE Trans. Power Electron.*, vol. 28, no. 12, pp. 5717–5727, Dec. 2013.

[7] M. Falahi, H.-M. Chou, M. Ehsani, L. Xie, and K. Butler-Purry, "Potential power quality benefits of electric vehicles," *IEEE Trans. Sustain. Energy*, vol. 4, no. 4, pp. 1016–1023, Oct. 2013.

[8] J. G. Pinto, V. Monteiro, H. Goncalves, and J. L. Afonso, "On-board reconfigurable battery charger for electric vehicles with traction-to-auxiliary model," *IEEE Trans. Veh. Technol.*, vol. 63, no. 3, pp. 1104–1116, Mar. 2014.

[9] T. Tanaka, T. Sekiya, H. Tanaka, M. Okamoto, and E. Hiraki, "Smart charger for electric vehicles with power-quality compensator on single-phase three-wire distribution feeders," *IEEE Trans. Ind. Appl.*, vol. 49, no. 6, pp. 2628–2635, Nov./Dec. 2013.

[10] R. Ferreira, L. Miranda, R. Araujo, and J. Lopes, "A new bi-directional charger for vehicle-to-grid integration," in *Proc. 2nd IEEE PES Int. Conf. Exhibit. Innov. Smart Grid Technol.*, Manchester, U.K., Dec. 2011, pp. 1–5.

[11] K. Mets, T. Verschueren, F. De Turck, and C. Develder, "Exploiting V2G to optimize residential energy consumption with electrical vehicle (dis)charging," in *Proc. IEEE 1st Int. Workshop Smart Grid Model. Simulat. (SGMS)*, Brussels, Belgium, Oct. 2011, pp. 7–12.

[12] S. Vandael, T. Holvoet, G. Deconinck, S. Kamboj, and W. Kempton, "A comparison of two GIV mechanisms for providing ancillary services at the University of Delaware," in *Proc. 4th IEEE Int. Conf. Smart Grid Commun.*, Vancouver, BC, Canada, 2013, pp. 211–216.

[13] H. Liu, Z. Hu, Y. Song, and J. Lin, "Decentralized vehicle-to-grid control for primary frequency regulation considering charging demands," *IEEE Trans. Power Syst.*, vol. 28, no. 3, pp. 3480–3489, Aug. 2013.

[14] M. C. Kisacikoglu, B. Ozpineci, and L. M. Tolbert, "Examination of a PHEV bidirectional charger for V2G reactive power compensation," in *Proc. IEEE Appl. Power Electron. Conf. Expo. (APEC)*, Palm Springs, CA, USA, Feb. 2010, pp. 458–465.

[15] O. Onar, J. Kobayashi, D. Erb, and A. Khaligh, "A bidirectional high-power-quality grid interface with a novel bidirectional noninverted buck-boost converter for PHEVs," *IEEE Trans. Veh. Technol.*, vol. 61, no. 5, pp. 2018–2032, Jun. 2012.

[16] K.-W. Hu and C.-M. Liaw, "On a bidirectional adapter with G2B charging and B2X emergency discharging functions," *IEEE Trans. Ind. Electron.*, vol. 61, no. 1, pp. 243–257, Jan. 2014.

[17] J. Choi, H. Kim, D. Kim, and B. Han, "High-efficiency grid-tied power converter for battery energy storage," *IEEE Trans. Power Del.*, vol. 29, no. 3, pp. 1514–1515, Jun. 2014.

[18] A. Arancibia, K. Strunz, and F. Mancilla-David, "A unified single- and three-phase control for grid connected electric vehicles," *IEEE Trans. Smart Grid*, vol. 4, no. 4, pp. 1–11, Dec. 2013.

[19] M. Kesler, M. C. Kisacikoglu, and L. M. Tolbert, "Vehicle-to-grid reactive power operation using plug-in electric vehicle bidirectional off-board charger," *IEEE Trans. Ind. Electron.*, vol. 61, no. 12, pp. 6778–6784, Dec. 2014.

[20] N. Mohan, T. M. Undeland, and W. P. Robbins, *Power Electronics: Converters, Applications, and Design*, 3rd ed. Hoboken, NJ, USA: Wiley, 2003.

[21] M. Mültin, C. Gitte, and H. Schmeck, "Smart grid-ready communication protocols and services for a customer-friendly electromobility experience," in *Proc. Smart Grid Workshop der INFORMATIK Gesellschaft für Informatik*, Sep. 2013, pp. 1470–1484.

[22] L. M. Miranda *et al.*, "Power flow control with bidirectional dual active bridge battery charger in low-voltage microgrids," in *Proc. 15th Eur. Conf. Power Electron. Appl. (EPE)*, Lille, France, Sep. 2013, pp. 1–10.

[23] *IEEE Recommended Practices and Requirements for Harmonic Control in Electrical Power Systems*, IEEE Standard. 519-1992, 2002.

[24] *Electromagnetic Compatibility EMC—Part 3-2: Limits—Limits for Harmonic Current Emissions (Equipment Input Current ≤ 16 A Per Phase)*, IEC Standard 61000-3-2, 2005.

[25] (Dec. 2012). *Featherweight Lithium-Ion Battery* [Online]. Available: http://www.cdtechno.com/pdf/lit/12_1093_0512.pdf

[26] M. Kesler and E. Ozdemir, "Synchronous reference frame SRF based control method for UPQC under unbalanced and distorted load conditions," *IEEE Trans. Ind. Electron.*, vol. 58, no. 9, pp. 3967–3975, Sep. 2011.

[27] H. Akagi, Y. Kanazawa, and A. Nabae, "Instantaneous reactive power compensators comprising switching devices without energy storage elements," *IEEE Trans. Ind. Appl.*, vol. 20, no. 3, pp. 625–630, Mar. 1984.

[28] R. Teodorescu, F. Blaabjerg, M. Liserre, and P. Loh, "Proportional-resonant controllers and filters for grid-connected voltage-source converters," *IEE Proc. Elect. Power Appl.*, vol. 153, no. 5, pp. 750–762, Sep. 2006.

[29] A. Timbus, M. Liserre, R. Teodorescu, P. Rodriguez, and F. Blaabjerg, "Evaluation of current controllers for distributed power generation systems," *IEEE Trans. Power Electron.*, vol. 24, no. 3, pp. 654–664, Mar. 2009.

[30] (Jul. 2014). *PSIM Tutorial: How to Use the Lithium-Ion Battery Model* [Online]. Available: http://www.powersimtech.com/wp-content/uploads/2013/04/Tutorial-How-to-use-Lithium-Ion-battery-model.pdf

[31] (Jul. 2014). *Lifebatt* [Online]. Available: http://www.lifebatt.com

Mithat C. Kisacikoglu (S'04–M'14) received the B.S. degree from Istanbul Technical University, Istanbul, Turkey, in 2005; the M.S. degree from the University of South Alabama, Mobile, AL, USA, in 2007; and the Ph.D. degree from the University of Tennessee, Knoxville, TN, USA, in 2013, all in electrical engineering.

Between 2007 and 2013, he was a Researcher with the University of Tennessee and a part-time Researcher with Oak Ridge National Laboratory, Oak Ridge, TN. In 2014, he joined Hacettepe University, Ankara, Turkey, where he is currently an Assistant Professor with the Department of Electrical and Electronics Engineering. His current research interests include electric vehicles (EVs), EV-grid integration, smart grid, renewable energy sources, and power electronic converters.

Dr. Kisacikoglu was the recipient of Post-Doctoral Return Fellowship Award from The Scientific and Technological Research Council of Turkey (TUBITAK) in 2013 to conduct research and development in the area of electric vehicle integration into the utility grid in Turkey.

Metin Kesler (M'12) received the M.Sc. and Ph.D. degrees in electrical education from Kocaeli University, Kocaeli, Turkey, in 2005 and 2010, respectively.

He was a Visiting Scholar with the University of Tennessee, Knoxville, TN, USA, in 2013, where he was also involved in several projects with the CURENT Engineering Research Center. He was also engaged in a project with the Power and Energy Group, Oak Ridge National Laboratory, Oak Ridge, TN, in 2013. He is currently an Associate Professor with the Department of Computer Engineering, Bilecik Seyh Edebali University, Bilecik, Turkey. His current research interests include power quality, plug-in electric vehicles, renewable energy systems, distributed energy resources, and active power filters.

Dr. Kesler was the recipient of the TUBITAK 2219 Post-Doctoral Research Award in 2013 to conduct research in the U.S.

Leon M. Tolbert (S'88–M'91–SM'98–F'13) received the B.E.E., M.S., and Ph.D. degrees in electrical engineering from the Georgia Institute of Technology, Atlanta, GA, USA, in 1989, 1991, and 1999, respectively.

He joined the Oak Ridge National Laboratory (ORNL), Oak Ridge, TN, USA, in 1991 and researched several electrical distribution projects with three U.S. Department of Energy Plants in Oak Ridge. He joined the University of Tennessee, Knoxville, TN, in 1999, and is currently the Min H. Kao Professor and the Head of the Department of Electrical Engineering and Computer Science. He is also a part-time Senior Research Engineer with ORNL and conducts joint research with the National Transportation Research Center (NTRC), Knoxville. His current research interests include areas of electric power conversion for distributed energy sources, motor drives, multilevel converters, hybrid electric vehicles, and application of silicon-carbide power electronics.

Dr. Tolbert was the recipient of the 2001 IEEE Industry Applications Society Outstanding Young Member Award and three prize paper awards from the IEEE. He was an Associate Editor of the IEEE TRANSACTIONS ON POWER ELECTRONICS from 2007 to 2012 and the IEEE POWER ELECTRONICS LETTERS from 2003 to 2006. He was the Chair of the Education Activities Committee of the IEEE Power Electronics Society (PELS) from 2003 to 2007. He is a member of several societies, such as the Industry Applications Society; the Industrial Electronics, Power, and Energy Society; and the PELS. He was also elected as a member-at-large to the IEEE Power Electronics Society Advisory Committee from 2010 to 2012, and he served as the Chair of the power electronics society Membership Committee from 2011 to 2012. He is a Registered Professional Engineer with the State of Tennessee.